Case Studies in Nondestructive Testing and Evaluation 6 (2016) 56–61

Contents lists available at ScienceDirect

Case Studies in Nondestructive Testing and Evaluation

www.elsevier.com/locate/csndt

Comparing cone beam laminographic system trajectories for composite NDT

Neil O'Brien [a,*], Mark Mavrogordato [a], Richard Boardman [a], Ian Sinclair [a], Sam Hawker [c], Thomas Blumensath [a,b]

[a] μ-VIS X-Ray Imaging Centre, University of Southampton, Highfield, Southampton, SO17 1BJ, UK
[b] ISVR, University of Southampton, Highfield, Southampton, SO17 1BJ, UK
[c] Nikon Metrology UK Limited, Tring Business Park, Icknield Way, Tring HP23 4JX, UK

ARTICLE INFO

Article history:
Available online 1 June 2016

ABSTRACT

We compare the quality of reconstruction obtainable using various laminographic system trajectories that have been described in the literature, with reference to detecting defects in composite materials in engineering. We start by describing a laminar phantom representing a simplified model of composite panel, which models certain defects that may arise in such materials, such as voids, resin rich areas, and delamination, and additionally features both blind and through holes along multiple axes. We simulate ideal cone-beam projections of this phantom with the different laminographic trajectories, applying both Simultaneous Iterative Reconstruction Technique (SIRT) and Conjugate Gradient Least Squares (CGLS) reconstruction algorithms. We compare the quality of the reconstructions with a view towards optimising the scan parameters for defect detectability in composite NDT applications.

1. Introduction

X-ray computed tomography (CT) is a widely accepted and applied method for non-destructive testing in the engineering community, applied across research and development, quality control, and post-failure analysis for engineered components. Since its introduction, the technique has been refined and developed considerably, with typical detector arrays improving from 80 × 80 pixels in the early days [1] to the order of several thousand pixels square today. Meanwhile, the introduction of new algorithms and computational techniques, such as general-purpose use of the graphics processing unit (GPGPU), has dramatically accelerated and enhanced the reconstruction process. By their nature, polymer matrix composites are widely used in planar forms in structural applications [2]. Whilst traditional micro-focus CT can provide high-resolution 3D visualisation of the structure of relatively small composite parts with aspect ratios that maintain broadly similar path lengths in all orientations during a scan, larger composite panels are less readily examined due to the limited space within a typical CT scanner and the likelihood of near-extinction of the X-ray beam along the long axis/plane of the sample, leading to photon starvation and artefacts in the reconstructed volume.

Several solutions to the problem of scanning larger composite panels and those with unfavourable aspect ratios have been explored, including dual-energy scanning using higher energies for the orientations with longer path-lengths [3], and

* Corresponding author.
E-mail addresses: nsob1c12@soton.ac.uk (N. O'Brien), mnm100@soton.ac.uk (M. Mavrogordato), rpb@soton.ac.uk (R. Boardman), is1@soton.ac.uk (I. Sinclair), Sam.Hawker@nikon.com (S. Hawker), Thomas.Blumensath@soton.ac.uk (T. Blumensath).

http://dx.doi.org/10.1016/j.csndt.2016.05.004

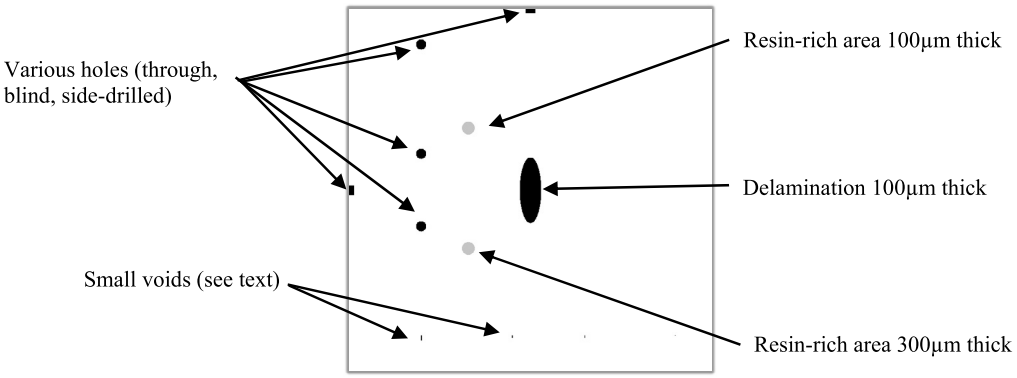

Fig. 1. Schematic layout of the phantom.

stacking samples within one CT scan to achieve more uniform path length and thus attenuation at all angles. A further key solution for imaging large planar composites is to use computed laminography (CL), which may employ any of several acquisition trajectories, combined with any of various reconstruction methods, many of which are adapted from CT. In avoiding a complete rotation of the sample in question, CL captures only a limited subset of the data that an ideal CT scan would contain, but makes feasible scans outside the scope of full CT. By utilising *a priori* knowledge in the reconstruction algorithm, high quality volume inspection is possible [4]. CL has been in use at synchrotron facilities for some time [5] and there is growing interest in cone beam laminography [6] which is practical using compact, laboratory-based sources.

In this paper we will introduce a phantom to represent a simplified composite sample with various defects, illustrate several laminographic system trajectories, and by comparing line-profiles through various reconstructions of the phantom, compare the quality of the results. This paper thus builds on the work of Rehak et al. [7] who analysed the influence of tilt angles on hat-shaped artefacts in laminography, using tomosynthesis and ART reconstruction algorithms.

2. Materials and methods

2.1. Description of the phantom

Our phantom consists of a cuboid, which measures 70.7 × 70.7 × 4 mm with a 100 μm voxel size. Simplified defects of interest in large engineering applications are modelled: we include through- and blind-holes along three axes as well as resin-rich areas of 100 μm and 300 μm thickness, and a delamination modelled as an air layer of 100 μm thickness on the central plane. We also included several smaller voids, ranging in size from a cube with 100 μm side length to a cuboid 200 μm × 200 μm × 1 mm. We adopted the elemental composition of the carbon fibre bundles and the epoxy from values given by Bliznakova et al. [8]. Using the attenuation data from the NIST database, we set the attenuation coefficients (per unit length) of the various parts of the phantom to 0.767 for the bulk material, 0.726 for the epoxy in the resin-rich regions, and 0 for the air regions; due to the simplifying assumptions we took, these are relative values in the sense that their ratios are significant but their absolute values are not. Whilst the features are spread throughout the thickness (z-axis) of the planar phantom, we show all features in a z-projection in Fig. 1.

2.2. Trajectories implemented

The simulated trajectories are illustrated schematically in Fig. 2 and consist of single axis linear motion, rotary laminography (CT with an inclined axis of rotation), linear raster scan with two orthogonal axes of motion, and swing or limited-angle CT scanning with rotation about one or two orthogonal axes (dual-axis annotated '2ax' in our results). We varied relevant parameters for each motion (i.e. the angular range covered the swing motion, the laminographic angle for the rotary, and the total displacements for the linear motions). We also considered both single- and double-sided illumination of the phantom, which could be implemented in a real system by several means including repositioning the sample relative to a source–detector pair, or potentially using multiple source–detector pairs.

2.3. Simulation techniques

We applied the ASTRA toolkit [9] which provides a number of routines for tomographic simulation and reconstruction development, including GPU-accelerated cone-beam forward projection and iterative reconstruction algorithms for arbitrary cone-beam acquisition geometries. We used both the SIRT and CGLS reconstruction methods as implemented in the ASTRA toolbox with a range of different iteration counts. We compare the line profiles recorded through certain features in our phantom with those through the reconstructed volumes for our chosen scan trajectories, in order to evaluate the relative

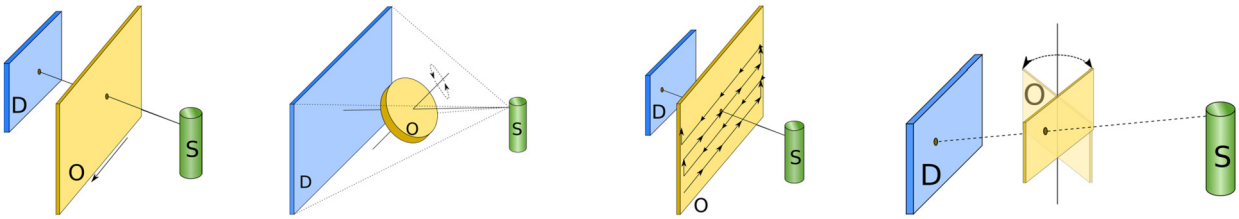

Fig. 2. Schematics of the scan trajectories we considered, from left to right: linear, rotary, linear raster, and swing (one axis of rotation is shown).

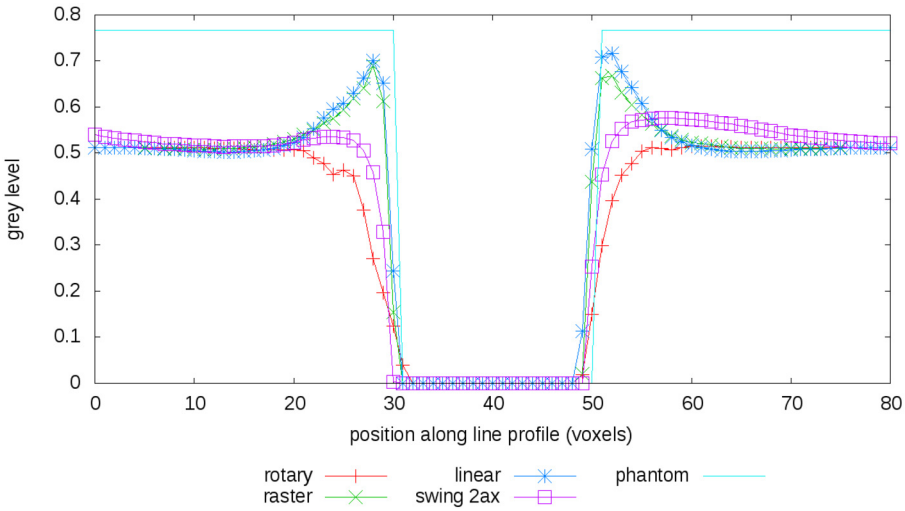

Fig. 3. Line profiles across through hole in x-direction for several trajectory types. 15 SIRT iterations were used, the specimen was illuminated from one side.

merits of each method to reveal flaws in laminar specimens. The simulations presented here take several simplifying assumptions including assuming a monochromatic point source, as well as not adding any artificial noise or detector faults to the simulated results. All output volumes were scaled such that the floating-point values were in the range $[0, 1]$ prior to taking the line profiles, ensuring comparability.

3. Results and discussion

3.1. Influence of trajectory type

In Fig. 3, we present line profiles through our phantom as well as through the reconstructed volume for each of the trajectories illustrated in Section 2.1. These results are all based on SIRT reconstructions using 15 iterations, and take a line profile across the through-hole feature, approximately 1/3 through the thickness of the volume. It can be seen that whilst all trajectories considered correctly reproduce the zero attenuation in the centre, the linear and raster trajectories have bright artefacts around the edge of the hole, which can also be seen in the left-hand part of Fig. 6, showing a slice through a raster scan reconstruction. The rotary trajectory does not give rise to a bright artefact, but suffers from the slowest gradient in grey-value across the edge of the feature. In Fig. 6 (centre and right illustrations) we show slice images through our reconstruction for two limited angle scans, illustrating the dependence of depth resolution on the chosen angle. The severity of hat-shaped artefacts can also be seen to vary with the chosen laminographic angle, in agreement with the findings of [7].

3.2. Influence of reconstruction parameters

In Fig. 4, we show line profiles through the second blind hole in our phantom, half-way down its depth. We compare the results for different iteration counts and reconstruction algorithms using the same projections, from our limited-angle simulation using two-sided scanning and a 2-axis swing motion between $\pm 45°$ about both axes. The overall feature contrast improves when increasing the iteration count, but the additional iterations also exacerbate the bright artefact arising at the edges of the hole. SIRT reconstructs the greyvalues of the phantom correctly in more places than CGLS but both methods produce a good qualitative match to the phantom. We note that for the detection of voids in an NDE application, this type of artefact may not pose a problem, but increasing iteration counts still incur the tradeoff of requiring increased processing time.

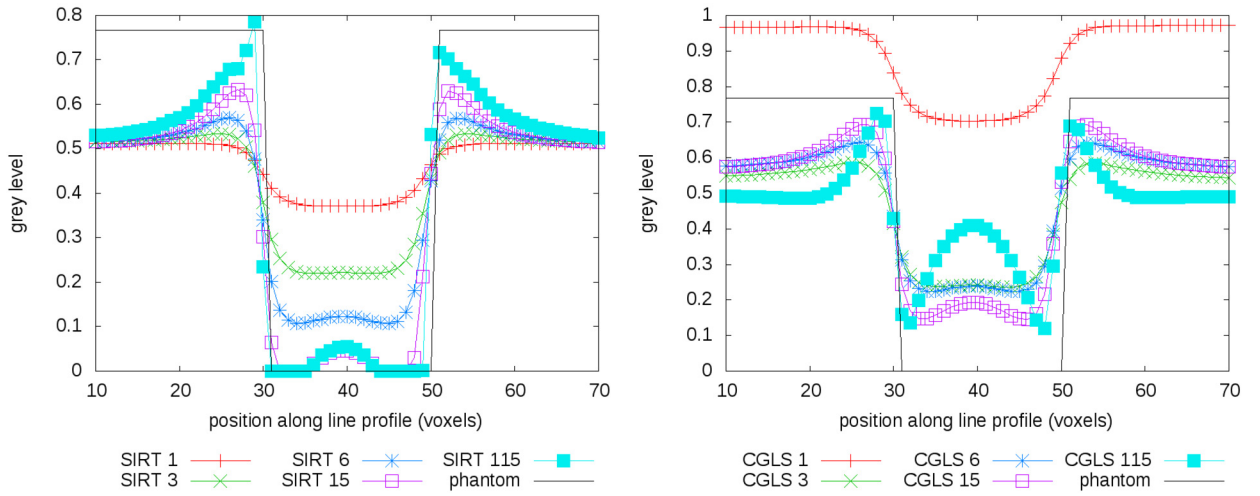

Fig. 4. Profiles along the *x*-direction of a blind hole in the reconstruction for various numbers of iterations of the SIRT (left) and CGLS (right) iterative reconstruction techniques. All results are from a 2-sided, 2-axis swing simulation using angular limits of ±45°.

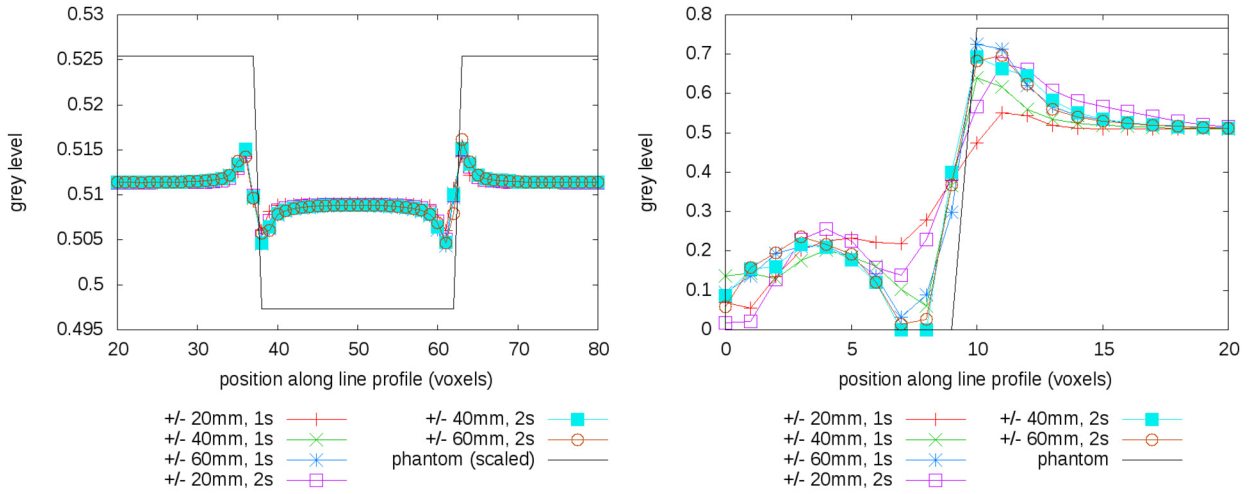

Fig. 5. Profiles along the *x*-direction through a resin-rich region (left plot) and side hole (right plot), showing influence of different total amounts of displacement and the difference between 1-sided (1s) and 2-sided (2s) raster scanning.

3.3. Influence of trajectory parameters

In this subsection we investigate the influence of the total displacement used in a raster scan on the quality of the resulting reconstruction. Fig. 5 compares raster scans for different total displacements. In each case, the cone-beam illuminates all parts of the phantom from a range of angles. With larger displacements, the outer edges of the phantom are illuminated by the rays over a greater range of angles than with smaller displacement values, improving the definition of the features investigated. In the left-hand plot, we have scaled the grey-values of the phantom

4. Discussion and conclusions

We have compared the ability of various laminographic trajectories to discern the features of our phantom. All the methods show promising results and those illuminating features from a larger range of angles typically give better resolution. The choice of reconstruction algorithm and iteration count is shown to be important. SIRT has provided results in better agreement with the phantom in these simulations, and for these data, 15 iterations achieves good feature definition without costing excessive compute time. In a real system we suggest that the iteration count should be decided empirically to optimise performance for specific acquisition setups, whilst the choice of trajectory will be influenced strongly by practical considerations such as the size of the specimen in relation to the space inside the scanner. Where practical, the dual-axis swing, or the rotary trajectory offer a good balance of limited edge-effects. If implemented such that the angular range

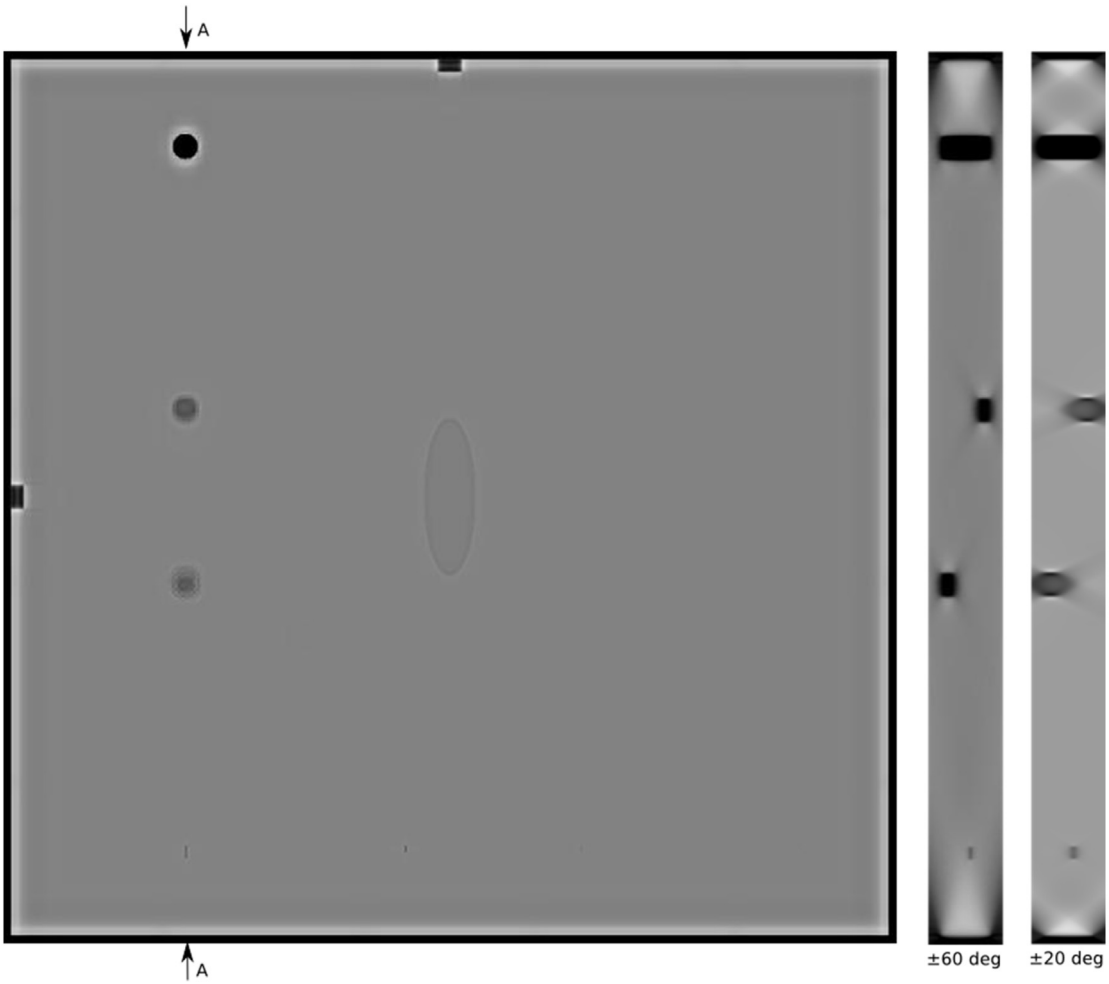

Fig. 6. (Left) slice through a 2-sided raster scan with 15 iterations of SIRT reconstruction showing reconstruction of central void, small voids, and various holes. (Right) slices through the thickness taken from 2-axis, 2-sided swing simulations along the path A–A, showing localisation of various defects in the thickness of the slice.

may be varied then good control over the tradeoff between angular range (which may influence scan time and collision risk/space requirement) and reconstruction quality may be achieved.

Acknowledgements

The authors gratefully acknowledge funding for ProjectCAN from Innovate UK, the UK's innovation agency through TSB grant 101804. The ProjectCAN consortium of QinetiQ, University of Southampton, University College London, Nikon, Axi-Tek, and Rolls Royce brings together world leaders from academia, the aerospace industry, and X-ray equipment manufacture. The simulations reported upon here have been discussed with consortium partners but the analysis and reporting of results was carried out entirely by the authors, who acknowledge the use of the IRIDIS High Performance Computing Facility at the University of Southampton. The authors also gratefully thank the anonymous reviewers for their helpful feedback.

References

[1] Beckmann EC. CT scanning: the early days. Br J Radiol 2006;79(937).
[2] Bull D, Helfen L, Sinclair I, Spearing SM. Multi-scale 3D imaging of carbon fibre laminate impact and compression after impact damage using computed tomography and laminography. In: ECCM15 – 15th European conference on composite materials. June 2012.
[3] Rouse JE. Characterisation of impact damage in carbon fibre reinforced plastics by 3D X-ray tomography. PhD thesis. Manchester, UK: University of Manchester; 2012.
[4] Helfen L, Myagotin A, Mikulík P, Pernot P, Voropaev A, Elyyan M, et al. On the implementation of computed laminography using synchrotron radiation. Rev Sci Instrum 2011;82(6).
[5] Helfen L, Xu F, Suhonen H, Cloetens P, Baumbach T. Laminographic imaging using synchrotron radiation – challenges and opportunities. J Phys Conf Ser 2013;425(19):192025.

[6] O'Brien NS, Boardman RP, Sinclair I, Blumensath T. Recent advances in X-ray cone-beam computed laminography. J X-Ray Sci Technol 2016. In press.
[7] Rehak M, Hassler U, Hanke R. Acquisition trajectories for X-ray tomosynthesis applied to planar samples. In: 2nd international symposium on NDT in aerospace. 2010.
[8] Bliznakova K, Dermitzakis A, Bliznakov Z, Kamarianakis Z, Buliev I, Pallikarakis N. Modeling of small carbon fiber-reinforced polymers for X-ray imaging simulation. J Compos Mater September 2014.
[9] van Aarle W, Palenstijn WJ, De Beenhouwer J, Altantzis T, Bals S, Batenburg KJ, et al. The ASTRA Toolbox: a platform for advanced algorithm development in electron tomography. Ultramicroscopy 2015;157:35–47.